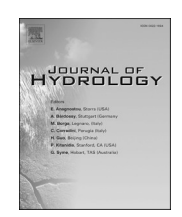


Contents lists available at ScienceDirect

Journal of Hydrology

journal homepage: www.elsevier.com/locate/jhydrol





Cascading effect of meteorological forcing on extreme precipitation events: Role of atmospheric rivers in southeastern US

Sourav Mukherjee, Ashok Kumar Mishra

Glenn Department of Civil Engineering, Clemson University, SC, USA

ARTICLE INFO

This manuscript was handled by Sally Elizabeth Thompson, Editor-in-Chief, with the assistance of Bellie Siyakumar. Associate Editor

Keywords: Atmospheric rivers Coastal SEUS Extreme precipitation Cascading effect Synoptic patterns Moisture advection

ABSTRACT

The past few decades have witnessed an intensification of extreme precipitation (EP) events triggered by atmospheric rivers (ARs), leading to massive flooding, highlighting the importance of studying the physical mechanisms associated with these types of events. This study aims to investigate the spatiotemporal evolution of ARs and related extreme precipitation (AR-EP) events, and the cascading effect of the synoptic-scale meteorological patterns on underlying processes in the Coastal States of the Southeastern United States (SUES) during the 1979-2019 period. The seasonal frequency of EP events associated with ARs suggests that more frequent AR-EP events occur during the colder months (November to April). In contrast, the AR-EP events are less frequent but more severe in the warmer months (May to October). A total of 12-15 AR-EP events, with severity exceeding the 99th percentile precipitation threshold, were observed during the 3-month overlapping seasons between November and April from 1979 to 2019 that affected Georgia, Florida, Alabama, and South Carolina. On the other hand, the average precipitation magnitude of the AR-EP events is relatively higher (55-90 mm/day) in the warmer months (May to October). To explore the cascading nature of relevant meteorological forcing on the physical processes that favor such events, we performed an event-centered composite analysis based on the top 100 severe AR-EP events observed during the extended cold and warm season, separately. It was observed that during the progression of the AR-EP events, the anomalies associated with composite mean sea level pressure (MSLP) and 850mb geopotential height (Z850) make a transition from the trough to ridge formation along with a south-eastward extension of Bermuda High in the cold season. The spatiotemporal evolution of these meteorological variables is found to have a cascading effect on the mode of moisture transport indicated by integrated vapor transport (IVT) and moisture availability shown by total column water vapor associated with the major AR-EP events. The warm season IVT field gets stronger 2-days before the AR-EP event occurrences indicating a continuous increase in moisture influx into the Gulf and Atlantic Coastal Plains. Similar strengthening of IVT is noted over the Gulf Coastal Plains during the cold season. A cascading effect is also noted for the moisture availability indicated by a significant increase in total column water vapor (TCWV) over the Gulf of Mexico 2 days before the events. Overall, the cold season AR-EPs are driven by relatively stronger dynamical systems indicated by greater IVT intensity. In contrast, the warm season AR-EPs are associated with a weaker IVT field, higher atmospheric instability, and more moist conditions.

1. Introduction

Recently, extreme precipitation events leading to massive floods have intensified in intensity, duration, and frequency in different parts of the world (Madsen et al., 2014; Mishra and Singh, 2010; Papalexiou and Montanari, 2019; Vu and Mishra, 2019). Much of this intensification is attributed to the acceleration of the hydrologic cycle caused by climate change (Schumacher and Rasmussen, 2020; Vu and Mishra, 2019; Wang et al., 2013; Wen et al., 2020), a considerable proportion of

which is associated with large-scale atmospheric features, such as atmospheric rivers (ARs) (Payne et al., 2020). Extreme precipitation and flooding associated with ARs have been reported in various parts of the globe (Kamae et al., 2017; Lavers et al., 2012; Lavers and Villarini, 2013a; Paltan et al., 2017; Ramos et al., 2015; Waliser and Guan, 2017), including the US (Barth et al., 2017; Debbage et al., 2017; Mahoney et al., 2016; Moore et al., 2011; Ralph et al., 2017; Ralph and Dettinger, 2011).

ARs are long, narrow corridors of strong poleward water vapor

E-mail address: ashokm@g.clemson.edu (A.K. Mishra).

 $^{^{\}ast}$ Corresponding author.

transport across the mid-latitudes (Neiman et al., 2008b; Newell et al., 1992; Zhu and Newell, 1998). They can be associated with the warm conveyor belt of extratropical cyclones and are often characterized by strong low-level winds. ARs are also responsible for approximately 90% of all pole-ward atmospheric water vapor transport across the mid-latitudes (Guan and Waliser, 2015; Zhu and Newell, 1998).

ARs have a varied extent of societal and eco-hydrological impacts, which range from beneficial to devastating. For example, ARs are one of the major contributors to the snowpack and freshwater resources in the arid portions of the southwestern US and responsible for 20–50% of the region's rainfall accumulation (Dettinger et al., 2011). ARs have been associated with 30% to 60% of the annual variability of total runoff, thereby impacting the seasonal availability of water resources in the west coast of the US (Chen et al., 2019). Landfalling AR storms are also recognized as potential drought busters in the Pacific Northwest by overcoming nearly 60–70% of all persistent droughts in the region (Dettinger, 2013).

ARs are even known for causing megafloods, often dubbed as "ARkstorms". These events impact thousands of square miles of urban and agricultural land across the US, disrupting millions of lives and causing massive economic damages (Porter et al., 2011). So far, more than 99% of all reported flood damages in the western US have been attributed to severe landfalling AR storms (Corringham et al., 2019). However, the impact of ARs is not limited to the west coast of the US. In the southeastern US, the major historical 1000-year flood event that occurred on May 1–2, 2010, has been attributed to ARs (Moore et al., 2011), which affected significant parts of Tennessee, Kentucky, and Mississippi. This specific series of ARs resulted in sustained precipitation (for 48 h) as high as 344.7 mm over Nashville, Tennessee, leading to flash flooding that resulted in 26 fatalities and caused \$2–\$3 billion of property damages (Moore et al., 2011).

Recognizing the potential socio-economic damages (e.g., agricultural and devastating flood damages) caused by the ARs in the SEUS, there has been a growing concern on the AR activities along the coastal southeast US (SEUS) (Gimeno et al., 2014). Many studies highlighted the possible association between major flood events in the central and southeastern US with strong water vapor transport into the SEUS from multiple moisture sources, such as the Caribbean Sea, the Gulf of Mexico, and the Atlantic Ocean (Dirmeyer and Kinter, 2010, 2009; Guan and Waliser, 2015; Lavers and Villarini, 2013b; Moore et al., 2011; Pfahl et al., 2013). An enhanced source of moisture originating in the Caribbean and the Gulf of Mexico can trigger large-scale flood events in the mid-western US during May-July (Dirmeyer and Kinter, 2010). The study detected a narrow fetch of moisture steering along the coast of Central America, extending from the Yucatan Peninsula and moving all the way upwards to the western Gulf of Mexico, where it connects with the Great Plains low-level jet (GPLLJ), a phenomena dubbed "Maya Express" (Dirmeyer and Kinter, 2009). Further, (Lavers and Villarini, 2013b) highlighted that much of the annual maxima floods from 1105 basins across the central US and reported that in 42.5% of the basins, more than half of the flood events are associated with ARs interacting with the SEUS. The major flooding event in the Ohio River Valley (May 1-2, 2010) was triggered by the ARs that originated from the eastern tropical Pacific and the Caribbean Sea (Moore et al., 2011). These studies highlighted the significant role of ARs in causing major flood events.

More recently, global (Guan and Waliser, 2015) and regional studies (Debbage et al., 2017; Mahoney et al., 2016; Miller et al., 2017; Rabinowitz et al., 2019) have provided crucial information on the climatological and synoptic aspects of ARs affecting the SEUS. More than 10% of AR landfalls, along the Gulf of Mexico and Gulf stream, contributed to more than 30% of the annual precipitation over most parts of the southeastern US (Guan and Waliser, 2015). During the period, 1980–2010, nearly 41% of the heavy precipitation events (>100 mm/day), and 52% of the spatially widespread heavy precipitation events (affecting 7000 km² area) in the southeastern US were associated with ARs (Mahoney et al., 2016). Focusing on persistent AR events with a

duration of at least 48 h, Debbage et al., 2017 reported that total $\sim\!40$ persistent AR events per year occurred along the SEUS coastline locations between 1979 and 2014. The study also highlights the potential role of Great Plains Jet (GPJ) and Caribbean Low-Level Jet (CLLJ) on the SEUS ARs, which happens to interact with the western Gulf of Mexico. Miller et al., 2017 investigated the synoptic patterns associated with minor-major flood events in the Pigeon River basin located downstream of the southern Appalachian Mountains over 5 years period. The synoptic patterns were found to reveal the role of a highly amplified slow-moving positively tilted trough formation that favored the AR-EP events over the region. Rabinowitz et al., (2019) selected 15 AR events between 2000 and 2015 across the Mississippi river valley and categorized their associated synoptic patterns as progressive troughs.

Multiple studies have highlighted the potential role of persistent atmospheric anomalies and structure of moisture transport for a better understanding of the behavior of AR-EP events (Dirmeyer and Kinter, 2010; Moore et al., 2011; Rabinowitz et al., 2019; Steinschneider et al., 2018; Zhu and Newell, 1998). More specifically, based on the available moisture sources and transport mechanism, it is possible to generate information related to the atmospheric conditions that are particularly moist and unstable at the same time. These synoptic conditions progressively intensify with time, triggering a sequence of favorable conditions for moisture transport and advection until they finally lead to the occurrence of heavy precipitation events. In such a context, "cascading effects" have been increasingly investigated to understand the sequence of interconnected processes that ultimately lead to extreme precipitation events. The cascading effects can be examined based on the evolution of meteorological features and moisture influx associated with the days before the AR-EP events. While previous studies explored the role of ARs in driving EP events over the SEUS, the potential influence of atmospheric anomalies on such processes was partly explored (Debbage et al., 2017; Mahoney et al., 2016). Furthermore, investigating the influence of atmospheric anomalies only for coastal interactions (Debbage et al., 2017) limits our understanding of such processes driving EP events across the SEUS region.

This study begins with determining the variation of EP events with respect to AR events. In the next step, the synoptic feature's space–time evolution is investigated to understand its cascading effect on the moisture transport that influenced the 100 most severe AR-EP events during the cold and warm season separately. More specifically, the primary objective of this study is to address the following questions:

(1) How are the AR events and AR-EP events distributed spatially and across different seasons in eight SEUS states (Florida, Alabama, Mississippi, Louisiana, Georgia, North Carolina, South Carolina, and Texas)?

(2) Is there a cascading effect of synoptic-scale meteorological forcing on the moisture availability and mode of advection associated with major AR-EP events observed in the region between 1979 and 2019?

The rest of the manuscript is organized as follows: Section 2 focuses on the data and methodology applied in the study; the results and relevant discussions are provided in Section 3; and finally, the summary of major findings and concluding remarks are provided in Section 4.

2. Data and methodology

2.1. Data

AR events are identified within the region bounded by latitudes 15° N to 45° N and longitudes -110° W to -55° W (hereafter referred to as the AR-detection region). Detection of ARs is performed by using specific humidity, and zonal and meridional wind fields for 20 pressure levels (between 1000 and 300 hPa inclusive), retrieved at 6-hourly time-steps for the period 1979–2019 from the high-resolution European Centre for Medium-Range Weather Forecasts Reanalysis 5 (ERA5) (0.25°x 0.25° grid resolution). The hurricane track data from 1979 to 2019 is obtained from the Atlantic Hurricane database (HURDAT2) to segregate the ARs

from the Tropical Cyclones (TCs). The HURDAT2 is available at 6-hourly intervals provided by the National Hurricane Center (available at https://www.nhc.noaa.gov/data/#tcr). Mean sea level pressure (MSLP) and 850 mbar geopotential height (Z850) are selected to study the synoptic patterns and their cascading effect on the moisture transport mechanisms. As such, 6-hourly Z850, total column water vapor (TCWV), and MSLP data were obtained from the ERA-5 at the native spatial resolution for the 1979–2019 period. While MSLP and Z850 are extensively used to define the large scale meteorological patterns that have a primary influence on extreme precipitation events (Barlow et al., 2019), TCWV is an essential component to assess the moisture availability associated with AR-EPs (Gimeno et al., 2012; Zhang et al., 2019).

The impact of ARs on the precipitation and EP events are studied for the SEUS region that includes the eight coastal states, namely, Alabama (AL), Georgia (GA), Louisiana (LA), Mississippi (MS), North Carolina (NC), South Carolina (SC), Texas (TX), and Florida (FL). The EP events are derived based on the daily observed precipitation dataset (1979-2019) obtained from the Climate Prediction Center (CPC) (https://www.esrl.noaa.gov/psd/), available at 0.5° horizontal grid resolution. The daily precipitation dataset provided by NOAA's CPC is produced from Global Unified Gauge-Based Analysis (from over 30,000 stations) with a daily time step (Chen et al., 2008). The CPC data has been validated against historical records and measurements at nearby stations, concurrent radar/satellite observations, and numerical model forecasts. To maintain consistency in spatial resolution across all datasets used in the study, we apply the Synergraphic Mapping System (SYMAP) (Maurer et al., 2002) to regrid the reanalysis dataset at the 0.5° CPC precipitation grid resolution. Reanalysis data available at 0.5°x0.5° is reasonable to capture the ARs and their potential influence on the EP events (Payne et al., 2020), and multiple studies investigated regional AR behavior at the same or coarser resolution (Debbage et al., 2017; Guan and Waliser, 2015; Lavers and Villarini, 2013b, 2013a; Mahoney et al., 2016; Paltan et al., 2017).

2.2. AR-Detection methodology

ARs are derived based on an AR-detection algorithm (Guan and Waliser, 2015), that incorporates the characteristics of vertically integrated vapor transport (IVT) within the lower troposphere at 6-hourly time-steps. The IVT measures the integrated moisture flux based on specific humidity and zonal and meridional wind characteristics. Considering the dual drivers of AR behavior (Integrated water vapor and wind), the IVT magnitude (or intensity) is increasingly used to diagnose ARs across various parts of the globe (Guan and Waliser, 2015; Mundhenk et al., 2016; Rabinowitz et al., 2019; Shields et al., 2018b; Waliser and Guan, 2017). The IVT intensity is calculated in a Eulerian framework by performing a mass-weighted vertical integration within the pressure levels ranging from 1000 to 300 hPa as follows:

$$IVT = \sqrt{\left(\frac{1}{g} \int_{1000}^{300} qu dp\right)^2 + \left(\frac{1}{g} \int_{1000}^{300} qv dp\right)^2}$$
 (1)

where g is the acceleration due to gravity (=9.81 m s $^{-2}$), q is specific humidity (kg kg $^{-1}$), u is zonal wind (m/s), v is meridional wind (m/s), and dp is the pressure difference (Pa) between adjacent pressure levels. The algorithm has been applied in many recent studies related to ARs (Debbage et al., 2017; Huning et al., 2019; Kim et al., 2018; Waliser and Guan, 2017). The reader is referred to Guan and Waliser (2015) for a detailed discussion on the AR-detection algorithm, the underlying motivation, sensitivity analysis, and its application. A brief discussion on the AR-detection procedure is summarized in Appendix A1 of the Supplementary Material.

It is important to note that, at any time-step, one or more AR landfalls may be detected provided all the requirements (see Appendix A1 of the Supplementary Material) are fulfilled. The algorithm detected a total of 14,992 landfalling ARs in the AR-detection region, which is 25.03% of

the total 59,900 six-hourly time-steps during the study period, 1979-2019.

2.3. AR event and AR-EP event identification

The impact of the ARs on the EP events is investigated for the grid cells (0.5°x0.5°) located within the eight SEUS states. Tropical cyclones are seldom identified as a common source of heavy rainfall in the southeastern United States (Knight and Davis, 2009; Mahoney et al., 2016). To assess the contribution from ARs alone, we removed the effect of Tropical cyclones (TC) from the analysis of AR-EP events. This is achieved by removing the AR days that coincide with the TC dates. Out of the detected landfalling ARs, we found 12,645 ARs occurring over at least one grid cell during the 1979-2019 period within or on the SEUS region boundary. AR duration is an important variable that controls precipitation magnitudes (Ralph et al., 2013). An AR event is identified based on the duration of ARs that occurred for three or more time steps (18 h or more) (Lavers and Villarini, 2013a; Ralph et al., 2013), and these AR events can generate extreme precipitation events (Lavers and Villarini, 2013a; Ralph et al., 2019, 2013). A similar methodology was used to examine the association between AR and extreme precipitation storms for the US's west coast (Lamiiri et al., 2017; Ralph et al., 2019) and Europe (Lavers and Villarini, 2013a). The AR-events are identified based on all the 12,645 landfalling ARs. Two ARs were considered independent (distinct) events if they were separated by more than 1 day.

Extreme precipitation events are determined by applying the peak-over-threshold method (Mishra and Singh, 2010; Mondal et al., 2020) for the SEUS grid locations. The daily extreme precipitation events are first identified based on the 95th (EP $_{95p}$) and 99th (EP $_{99p}$) percentile threshold, separately. These percentiles are calculated for all non-zero daily precipitation totals observed during the whole time-period, 1979–2019. Finally, an AR-EP event is defined as the extreme precipitation event observed during or one day after an AR-event. This concept of AR events facilitates the association with the daily precipitation data and have been extensively used in previous studies (e.g., Guan et al., 2010; Huning et al., 2019; Lavers and Villarini, 2013a, 2013b; Neiman et al., 2008a). It should be noted that throughout the manuscript, the AR-EP events evaluated based on the 95th (99th) percentile threshold are referred to as AR-EP $_{95p}$ (AR-EP $_{99p}$).

2.4. Composite analysis

An event-centered composite analysis is performed to examine the evolution of the synoptic meteorological features and moisture availability and advection. So far, event-centered composite analysis has been extensively used in numerous studies to explore the relevant synoptic-scale meteorological features associated with a specific meteorological event (Barlow et al., 2019).

The event-centered composite analysis is performed based on the top 100 severe AR-EP $_{99p}$ events, selected separately for the extended warm (May-October) and cold (November-April) seasons. Firstly, the AR-EP $_{99p}$ time-series for individual grids (across the SEUS region) for a given season (warm and cold) are selected to form a matrix, with the dates and the corresponding AR-EP magnitude representing the columns of the matrix. The daily AR-EP magnitudes are then arranged in a decreasing order to identify the top 100 AR-EP events with unique dates for the composite analysis. The selected event days are used to obtain the seasonal anomalies in composites of meteorological variables at zero-day, 2-day, and 5-day lags. This approach is useful for exploring the sequence of interconnected processes (cascading effect) driving the top 100 severe AR-EP events.

More specifically, seasonal anomalies in the daily mean composites of the meteorological variables (MSLP, Z850, and TCWV) are calculated at every grid location by subtracting the mean of daily values coinciding with the time of occurrence of the selected top 100 AR-EP events from the long-term mean for the 1979–2019 period. Furthermore, a two-

sample Kolmogorov-Smirnov Test (KS-Test) is performed to determine the statistical significance (at 95% confidence level) of the anomalies at every grid location. To determine the moisture advection into the region, we calculate the composite mean of the daily IVT field during which the top 100 AR-EP events are observed for every grid location. Finally, to assess their temporal evolution over time, each of these composite and composite anomalies are also calculated for 5 days and 2 days prior to the occurrence of the top 100 AR-EP events. A similar approach has been adopted by Ridder et al. (2018) to investigate the temporal evolution of atmospheric conditions associated with AR-influenced EP along the Dutch coast.

3. Results and discussion

3.1. Spatial distribution of EP and AR events in SEUS

EP events generally affect a varied range of areas (smaller to larger) across the SEUS throughout the year (Moore et al., 2015). To understand the spatial patterns associated with EP and AR events in the SEUS, we constructed spatial maps showing the number of EP_{95p}, EP_{99p}, and only AR (after removing the TCs) events. Fig. 1(a, c, and e) depicts the spatial distribution of the annual event counts of EP_{95p}, EP_{99p}, and AR, respectively, for the 1979–2019 period. The results are further summarized as boxplots based on the eight SEUS states shown in Fig. 1 (b, d, and f).

Fig. 1(a-d) show that except for Texas, all other states are affected by $11{\text -}16$ (2–5) EP_{95p} (EP_{99p}) events per year. A homogenous spatial pattern is noted for the EP_{95p} event counts across most parts of the SEUS region, eastward of Texas. The EP_{99p} event counts, however, vary considerably across the SEUS, with a higher number of events clustered in the eastern Gulf coastal plains and the western part of the Florida peninsula. This is also indicated by the boxplots in Fig. 1(d) that show a comparatively greater (3–5) number of EP_{99p} events per year observed over Georgia, Florida, Alabama, and South Carolina.

Fig. 1(e-f) shows that the rate of AR activities is found to be relatively higher along the Atlantic coastal plain of the SEUS. More than 12 AR events are observed per year over the southeastern Appalachian range extending southwards along the Atlantic coastal plain up to the southern tip of the Florida peninsula. This spatial distribution is mirrored by the boxplots depicted for the eight SEUS states, as shown in Fig. 4 (f). A relatively greater (12–15) number of AR events per year affects the easternmost states, including larger portions of South Carolina, Florida, North Carolina, and Georgia. Furthermore, the spatial distribution of AR event counts closely matches the spatial pattern exhibited by the EP95p events, especially along the eastern coast of NC, SC, Georgia, and Florida located along the east side of the Appalachian range.

Interestingly, the regions showing a higher frequency of AR events are found to be located along the trajectory of the Sub-tropical Low-level Jet streams (SLLJ) attributed to the Atlantic warm pool (Wang and Lee, 2007). The SLLJ represents a persistent air mass influx into the subtropics and possibly supplies a significant share of moisture into the region combined with ARs that typically act along the CLLJ or westerlies in the region. This favors the influx of moisture into this region resulting in most AR activities along the coast of Atlantic coastal plains.

3.2. AR-EP characteristics in SEUS

ARs have been typically associated with EP events across different parts of the globe (Dettinger, 2011; Gimeno et al., 2014; Guirguis et al., 2019; Mahoney et al., 2016; Moore et al., 2011; Rutz et al., 2013; Tsuji and Takayabu, 2019; Valenzuela and Garreaud, 2019). The pronounced temporal and location-dependent behavior exhibited by the number of AR event occurrences (as seen earlier) is likely to be reflected in the EP occurrences driven by the ARs, which is the focus of this analysis. As such, using daily observations of precipitation accumulation from CPC, the AR-EP events are identified at every grid point based on a peak-overthreshold approach, as discussed in section 2.4. Figure S1 shows the geographical distribution of 95th and 99th percentile thresholds based

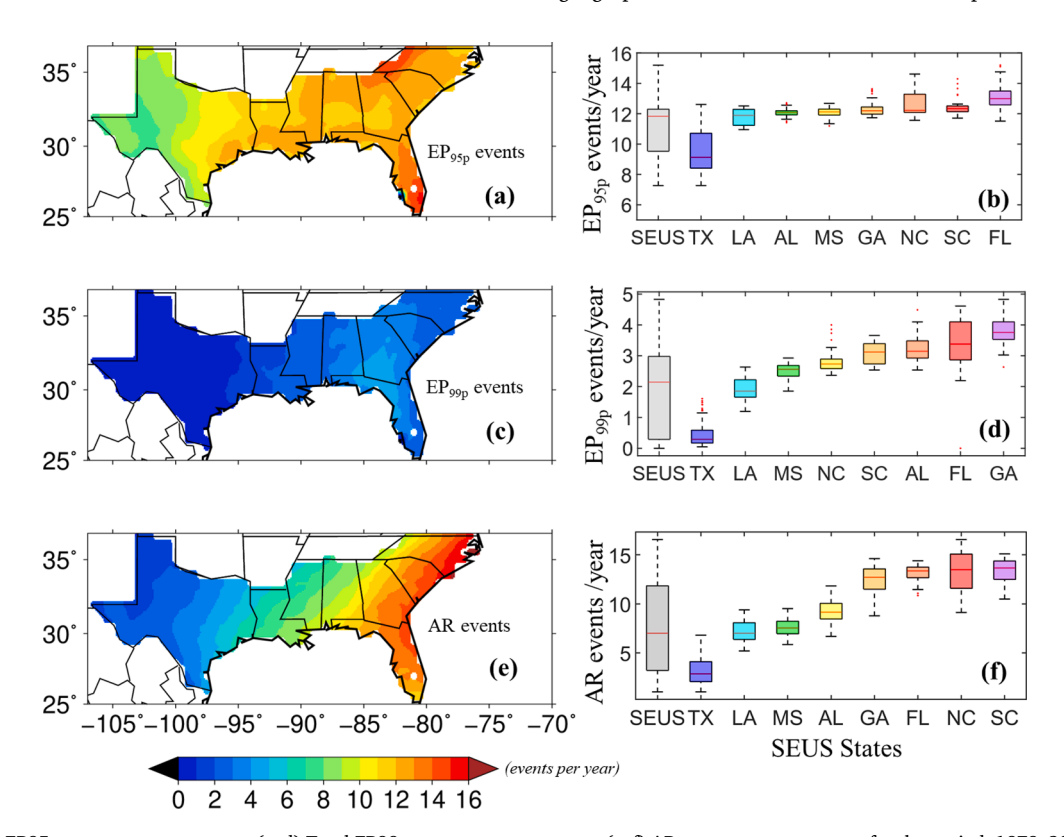


Fig. 1. (a-b) Total EP95p event counts per year, (c-d) Total EP99p event counts per year, (e-f) AR-event counts per year for the period, 1979–2019 (after removing the TCs).

on which the peak-over-threshold methodology is applied to the daily precipitation totals.

In this section, we explore mainly two characteristics of AR-EP events, the spatial distribution of the frequency (per year) of the AR-EP events and the seasonal variation of the frequency and the average magnitude of these events across the SEUS region. The annual frequency of AR-EP events is examined at each grid point to identify any locationdependent behavior revealed by the observed AR-EP events during the selected period. Fig. 2(a-d) shows the spatial distribution of the annual frequency of AR-EP95 and AR-EP99 events for the SEUS region and eight states for the 1979-2019 period. In addition to that, we also examine the precipitation characteristics (spatial distribution and magnitude) across the SEUS region for selected ARs observed during 3rd and 4th May 2010due to their association with large scale flooding (Mahoney et al., 2016), as shown in Fig. 2(e-f). The seasonal variations of the total AR-EP event count and average magnitudes for the 1979-2019 period are depicted by heatmaps as shown in Fig. 3. The seasonal variations are supposed to reveal any temporal dependence exhibited by AR-driven EP events and their severity in the SEUS and including states.

As shown in Fig. 2(a-b), the spatial patterns depicted by the annual frequency of AR-EP events are also in close agreement with that obtained for the EP and AR-events (Fig. 1). About 3–5 AR-EP $_{99p}$ and at least 1–2 AR-EP $_{99p}$ events per year are found to occur in the eastern part of the SEUS region, with the greatest number of events occurring primarily in the sub-tropical region along the northwestern coast of the Florida peninsula and south of Georgia. The higher rate of AR-EP events in these regions is also reminiscent of the fact that about 90% of the total water vapor flux is attributed to ARs located within the sub-tropics (Ralph

et al., 2004; Zhu and Newell, 1998). These results are further reflected by the boxplots that show the greatest number of AR-EP events occurred in Florida and Georgia (Fig. 2(c-d)). These results are concordant with the spatial pattern exhibited by the EP_{99p} event counts for these regions (Fig. 1(d)).

Fig. 2(e–f) shows the spatial pattern and severity of the AR-EP events that cause extreme socio-economic damages in the past. We selected two consecutive ARs observed on 3rd and 4th May 2010. It can be noted that these ARs are associated with a daily precipitation total of more than 100 mm, observed across the junction between the Gulf and Atlantic coastal plain of the SEUS (Fig. 2(f)). Previous studies have reported these ARs were associated with major historic flooding in the SEUS (Mahoney et al., 2016; Moore et al., 2011).

To explore the temporal dynamics of the AR-EP event characteristics, we examine the seasonal variation of the total event counts and average precipitation magnitude for the SEUS region and the eight including states for the 1979–2019 period. The seasonal variation of total AR-EP event counts and average precipitation magnitude are examined based on the seasons defined by a 3-month overlapping windows for all 12 months. The 3-month overlap allows for scaling the seasons to represent uniform 90-day seasons. Based on this criterion, we obtained the regional averages of seasonal counts of AR-EP_{95p} and AR-EP_{99p} events and the corresponding average precipitation magnitudes as illustrated by the heatmaps in Fig. 3(a-b) and Fig. 3(c-d), respectively.

A marked cold season dependence is noticeable in the total AR-EP event occurrences. A greater number of events is noted over Georgia, Florida, Alabama, and South Carolina during the October-November-December (OND), November-December-January (NDJ), December-

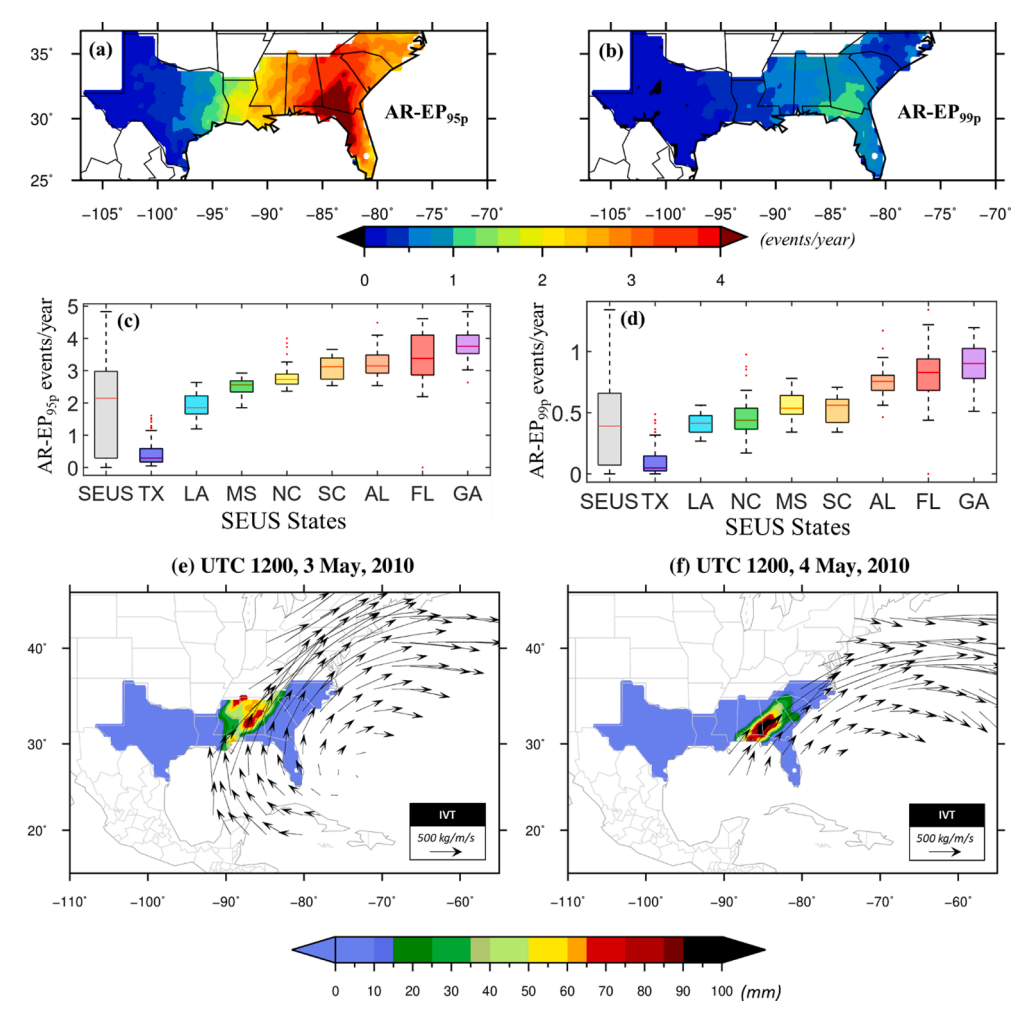


Fig. 2. (a–b) Spatial map showing the total number of (a) AR-EP_{95p} and (b) AR-EP_{99p} events observed per year during the 1979–2019 period over the SEUS region, (c–d) boxplots showing the spatial distribution of (c) AR-EP_{95p} and (d) AR-EP_{99p} event counts per year for the period 1979–2019 for the eight states of the SEUS region, and (e–f) spatial map showing the total precipitation magnitude (mm) and the IVT vectors for the ARs identified during the 3rd and 4th May 2010. The intensity of the IVT is represented by the length of the IVT vectors.

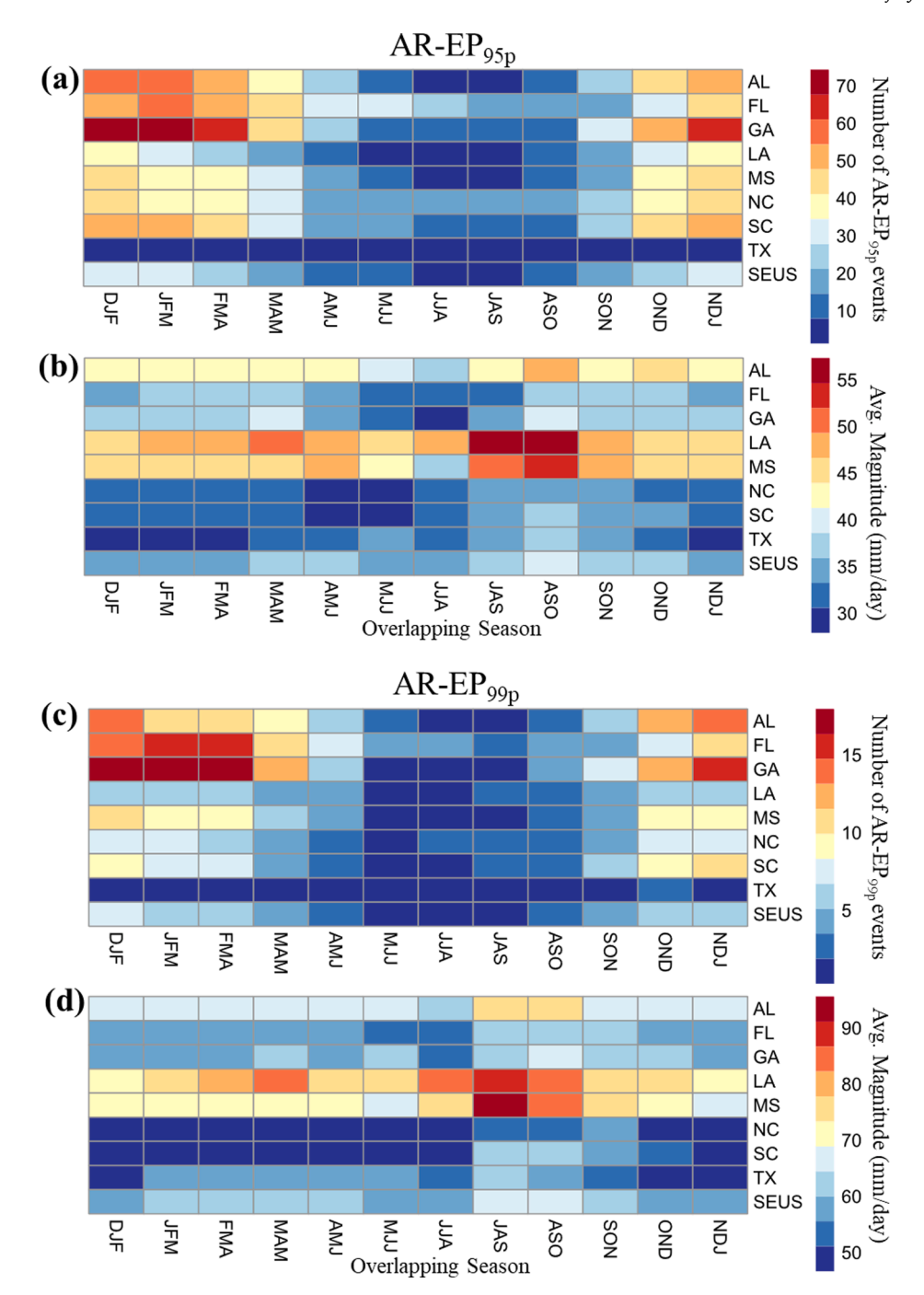


Fig. 3. The heat maps (a) show the total number and (b) average magnitude of AR-EP₉₅ events for the overlapping seasons during the period 1979–2019, (c, and d) same as in (a, and b) but for AR-EP₉₉ events.

January-February (DJF), January-February-March (JFM), February-March-April (FMA), and March-April-May (MAM) season (Fig. 3(a, and c)). These regions show a total of more than 50 AR-EP_{95p} and 12–15 AR-EP_{99p} events in each overlapping season between November and April during the 41-year period (1979–2019). Only a few AR-EP events (less than 5–10 events) are found to occur during the extended warm season months (April-May-June (AMJ) to September-October-November (SON)) over the entire SEUS region. These findings are in close agreement with previous studies that suggest the possible contribution of ARs to more frequent rainfall events in the SEUS with a greater influence observed predominantly during the cold season (Debbage et al., 2017; Mahoney et al., 2016).

The anomalously high AR-EP counts, markedly noticeable during the

months of the extended cold season (November-April), is generally attributed to the large-scale moisture availability and synoptically driven strong transport mechanisms acting simultaneously during the winter/transition months in the region (Mahoney et al., 2016; Moore et al., 2011). In addition to that, a considerable decrease in the AR-EP event count is notable from spring to summer seasons for most of the regions. As reported by previous studies, this is due to the spring to summer decrease in the large scale and persistent mesoscale convective systems in the west of the Appalachian Mountains, as well as due to the smaller number of ARs interacting with the CSE-US region during the warm season (Debbage et al., 2017; Parker and Ahijevych, 2007; Rickenbach, 2018).

In contrast, the average precipitation magnitude of the AR-EP_{95p} and

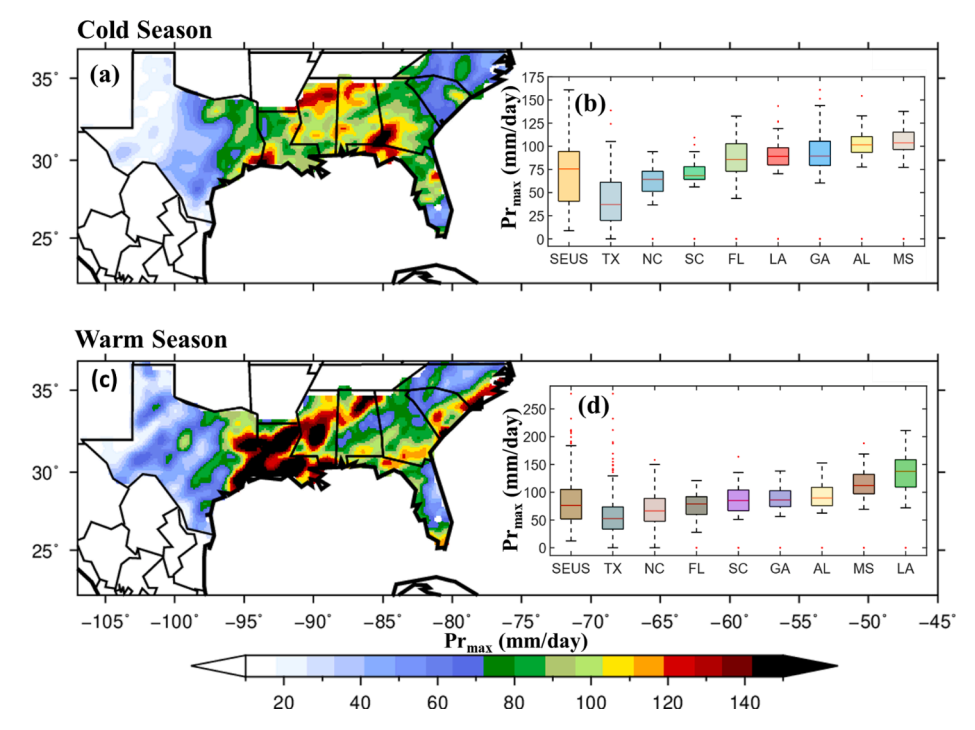


Fig. 4. (a) Spatial map and (b) box plots showing the geographical distribution of maximum AR-EP magnitude for the top 100 severe AR-EP days during the extended cold (Nov-April) season for the 1979–2019 period, and (c), and (d) same as in (a), and (b), respectively, but for the extended warm (May-Oct) season.

AR-EP $_{99p}$ events is found to be more than 55–90 mm/day in Louisiana and Mississippi in July-August-September (JAS) and August-September-October (ASO) seasons. The cold season AR-EP $_{95p}$ and AR-EP $_{99p}$ events, on the other hand, are found to be characterized by only 35–60 mm daily total precipitation in the SEUS region. These results indicate that the AR-EP events in the SEUS region are more severe during the warm season than those observed in the cold season. The association between ARs and more severe EP events in the warm season could be related to higher atmospheric instability and moisture availability (Moore et al., 2015).

Overall, this seasonal-count cycle seems to be equivalent to the annual IVT cycle, reported for the West Coast of the US (Mahoney et al., 2016). The largest vapor transport occurring during the winter and markedly decreasing during the summer can be attributed to the weak transient baroclinic instability during the warm season (Mahoney et al., 2016). This is also in agreement with the previous findings that associate ARs with the winter planetary wave number 4–5, a wavenumber typically associated with the synoptic-scale Extratropical Cyclones in the Northern Hemisphere (Zhu and Newell, 1998). Besides, the Extratropical Cyclones that are most prevalent during the winter, are climatologically associated with more number of ARs from October to March. (Mahoney et al., 2016).

3.3. Cascading effect of synoptic patterns on moisture availability and transport

This section explores the synoptic-scale evolution of atmospheric patterns, moisture availability, and transport mechanisms associated with AR-EP events during the extended warm (May to October) and extended cold (November to April) season. Composites of Z850, MSLP, IVT, and TCWV (refer to Section 2.4 for methodology) are generated 2 and 5 days prior and during the day of the top 100 severe AR-EP events observed during each season. It is expected that such spatiotemporal evolution can help to explore the sequence of events, thereby revealing any cascading effect (if present) of these synoptic-scale meteorological patterns on the moisture availability and transport associated with the top 100 severe AR-EP events. Moreover, the extended warm and cold season months (considered in the composite analysis) are chosen

objectively to meet the criteria of maximum seasonal dependence of AR-EP event occurrence and severity in the SEUS region (Fig. 3). While such seasonal dependence of the severity of the AR-EP events is noted in the May-October months of the extended warm season for Louisiana and Mississippi, for most of the other states a greater number of AR-EP events are observed during the extended cold season months (November-April) (Fig. 3).

The spatial distribution of the maximum daily precipitation totals during the selected top 100 AR-EP event days is illustrated in Fig. 4. Interestingly, for the top 100 severe cold (warm) season, AR-EP events are found to exceed a severity of 150 (200) mm/day in the SEUS region, mostly clustered over the eastern Gulf coastal plains (western Gulf and Atlantic coastal plains). The most severe cold season AR-EP events affected Mississippi, Georgia, and Alabama, whereas Louisiana and Mississippi experienced the most severe warm-season AR-EP events (Fig. 4 (b, and d). These results are in close agreement with the spatiotemporal characteristics of the AR-EP events during the warm and cold seasons depicted earlier in Fig. 3. We use the top 100 severe AR-EP event days observed for the warm and cold seasons in the subsequent composite analysis.

Firstly, we examine the spatiotemporal evolution of synoptic-scale meteorological patterns relevant to the occurrence of the top 100 severe AR-EP event days by using daily composite anomaly maps of Z850 and MSLP for the warm and cold seasons. Finally, we investigate if the sequence of spatiotemporal behavior exhibited by such atmospheric patterns shows a cascading effect on the spatiotemporal evolution of moisture advection and source identification associated with the top 100 AR-EP events in the region. For that, daily mean composite maps of the IVT field and daily mean composite anomaly map of TCWV are constructed for both seasons. The obtained results are discussed in the following sub-sections.

(a) Synoptic-Scale Meteorological Patterns:

Fig. 5 (a–c) and Fig. 5 (d-f) depict the spatiotemporal evolution of anomalies in composites of MSLP (shading) and Z850 (contour) for the cold and warm season, respectively, 5-days (indicated by "-5days") and 2-days (indicated by "-2 days") prior, and on the day (indicated by "0 days") the events are observed. It can be noticed that the composite

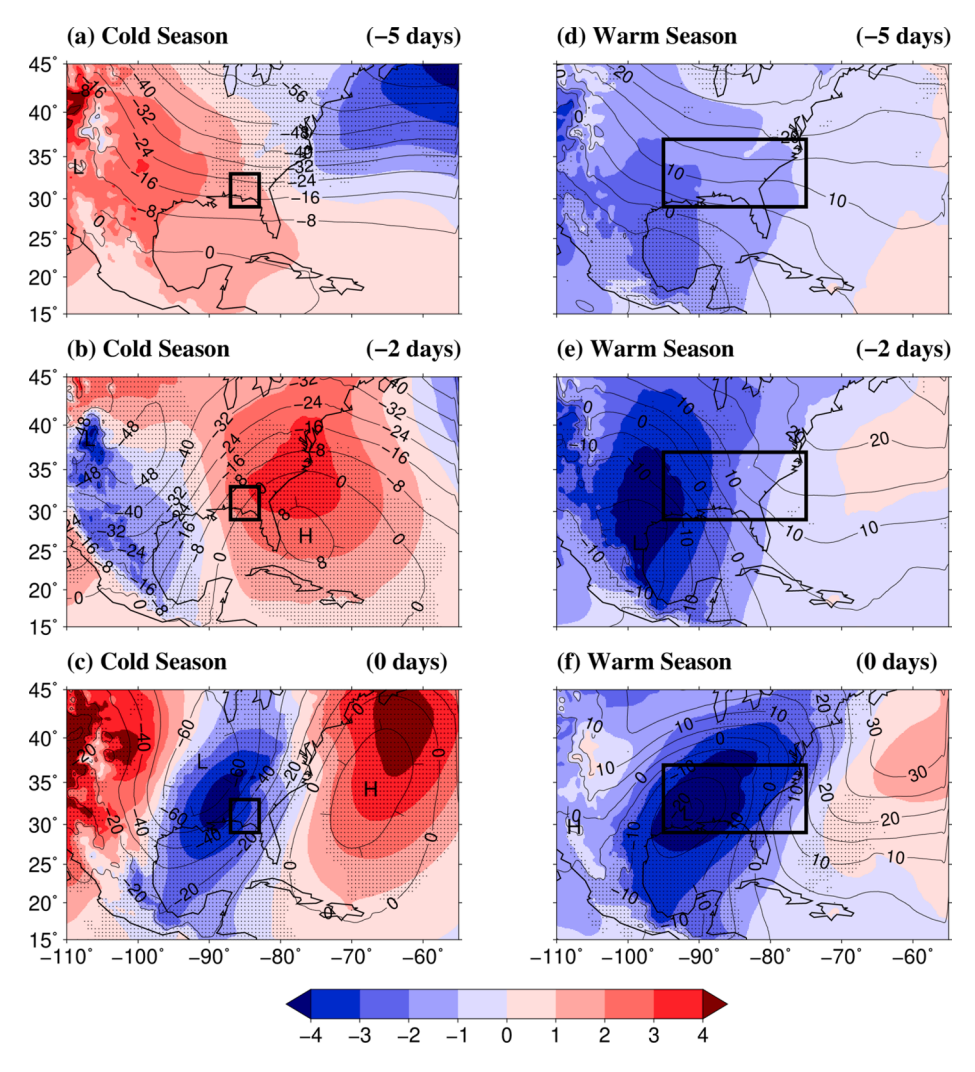


Fig. 5. Spatial map showing spatiotemporal evolution of (a-c) anomalies in composites of MSLP (shading; units hPa), and Z850 (contours; units: m) for cold (NDJFMA) season average centered on (a) 5 days before, and (b) 2 days before, and (c) on the day the top 100 severe AR-EP events are observed during the cold season; the location of the local maxima (minima) in Z850 anomaly are marked by the letter, "H" ("L"), (d–f) same as in (a–c) but for warm (MJJASO) season; striplings mark the grid points for which the anomalies in MSLP are found to be statistically significant (at 95% confidence level) based on the two-sample KS-test. The region corresponding to the top 100 severe AR-EP events is defined by the rectangle (black).

anomalies indicate a synoptic-scale meteorological pattern that exhibits a marked cascading behavior over the region during 5 to 0 days from the time of occurrence of the warm and cold season AR-EP events.

The Z850 anomaly contours for the cold season AR-EP suggest several trough and ridge (shown by positive anomalies) formation from 5 and 2 days before the AR-EP event occurrences. The trough formation (shown by negative anomalies) occurs along the south of the Rockies to the Great Plains region, while the ridge formation occurs along the east of the Appalachian along the Atlantic coastal plains. Much of the Central Plains and the Gulf Coastal plains are found to correspond to the transition region from the trough to the ridge, which is more pronounced on the day of the events (0-days; Fig. 5(c)). Such transitions are typically characterized as a zone of enhanced geostrophic winds (winds associated with the middle latitudes aloft in the troposphere), making the region more vulnerable to ARs (Moore et al., 2011; Pasquier et al., 2019).

MSLP anomalies suggest an eastward extension of the Bermuda high stretching southwards as the day progresses from 2-days before the day, the events are observed. This phenomenon is typical of the North Atlantic region and is mainly observed during the winter months. The extension of Bermuda High acts as a block that prevents the frontal systems from curving out to the Atlantic Ocean, which instead steers into the Gulf of Mexico. This also allows the SLLJ streams to dip further south into the SEUS region, sometimes bringing wintry storms with it, thus marking the importance of the confluence of SLLJ and ARs in relation to the AR-EP events in SEUS region. The region is characterized by a weak pressure gradient 5 days before the occurrence of the events. This

pressure gradient, however, becomes stronger 2 days before the onset of the observed events. Interestingly, on the days of the events (0 days), the low-pressure anomaly can be seen to intensify and shift southeast, covering the locations where the EP events are mainly observed (defined by the rectangular bounded region in Fig. 5). In addition to that, the cold season synoptic patterns depict a strong pressure dipole with a strong low-pressure center sandwiched between the extended Bermuda High and abnormal high pressure existing over the western US. This low-pressure system in the region is likely to favor the advection of moisture from the southerly winds.

Similarly, the Z850 anomaly contours for the warm season AR-EP depict an intense low-pressure center, particularly over much of the SEUS. More importantly, the low-pressure center can be seen to intensify over the western Gulf-coastal plains and stretch slightly eastwards between 5 and 2 days before the events. This low-pressure center remains stationary over the region and intensifies until the day of the events, covering much of the Gulf coastal plain. This particular structure is indicative of cut-off lows that are often characterized by the presence of a height cap limiting the vertical movement of an air parcel, which, when moist, increases the chances of heavy rainfall (Barbero et al., 2019), a phenomenon reported by (Moore et al., 2011) in connection with the severe flooding across the Ohio river basin on May 1–2, 2010. In addition to that, the MSLP pattern exhibits an intense low-pressure anomaly in the Gulf coastal plains, persistent from 2-days before the day of the events. This type of persistent low-pressure structure is indicative of slowly varying background circulations that favor deep moist convection leading to more severe warm-season EPs (Figs. 3 and

4) in the region (Moore et al., 2015; Nie and Fan, 2019).

(b) Moisture Availability and Transport:

To examine the cascading effect of the synoptic-scale meteorological patterns on the moisture availability and transport mechanism associated with such AR-EP events, we calculated the composite mean of the IVT field and anomalies in the composite mean of TCWV for the same event days for the cold and warm season. The composite maps for assessing the moisture availability and transport are presented in Fig. 6.

For both cold and warm season, intense IVT field over the strong low-pressure region in the Gulf Coastal Plains (where the AR-EP events are observed as depicted previously in Fig. 4) can be observed to develop 2 days before the event occurrences, which amplifies substantially (IVT intensity $>400 \, \text{kg/m/s}$) on the days when these events are observed. A dominant role of CLLJ and strong westerlies associated with the SLLJ is

also notable from the IVT field for the cold season ARs. The CLLJ can be seen to cross the Yucatan Peninsula that phases with the strong SLLJ steering along the west coast of the Gulf of Mexico, bringing moisture to the region, particularly over the lower Mississippi river basin. For both seasons, the IVT field indicates that the ARs show a tendency to curve out to the center of the extended Bermuda-Azores High towards the eastern coast of Europe. This also explains the relatively higher number of AR landfalls along the Atlantic coastal plains, as indicated by the spatial distribution of AR events in Fig. 1(e). Such moisture advection process conforms with the evolution of synoptic meteorological patterns exhibited by the MSLP composite anomalies presented in Fig. 5 (a–c). Along the east coast of the Gulf of Mexico, the CLLJ alone can be seen to dominate the advection of moisture into the region, with the Caribbean Sea and the Atlantic Ocean being the primary sources of moisture.

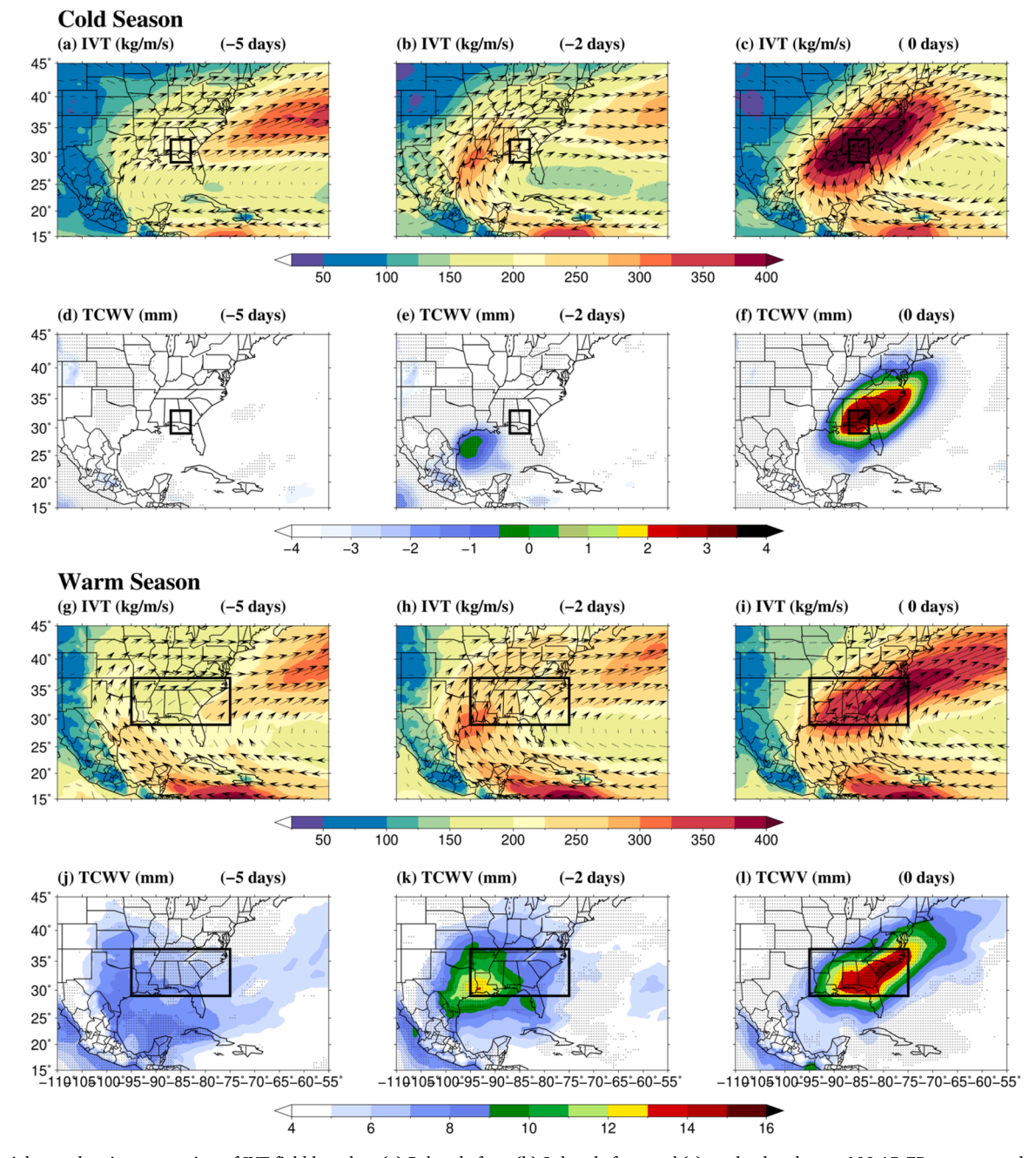


Fig. 6. Spatial map showing composites of IVT field based on (a) 5 days before, (b) 2 days before, and (c) on the day the top 100 AR-EP events are observed during the cold (Nov-April) season, (d–f) same as in (a–c) but for composite anomalies in TCWV, (g–i) same as in (a–c) but for warm (May–Oct) season, and (j–l) same as in (d–f) but for the warm season. The anomalies are estimated based on the cold or warm season average, and the striplings indicate the grid points where statistically significant (95% confidence level) anomalies are obtained. The region corresponding to the top 100 severe AR-EP events is defined by the rectangle (black).

Moreover, the temporal evolution of the availability of moisture (represented by the significantly positive anomalies in TCWV) can be seen to mimic that of the IVT magnitude over the region of interest and the surrounding area of the Southeast coastal plains.

For the warm season, the IVT field associated with the ARs is relatively weaker but spread across a wider area, including both the Gulf and the Atlantic coastal plains (Fig. 6(i)). The advection of moisture into the region can be primarily associated with the CLLJ bringing plumes of moisture from the Caribbean Sea and the Atlantic Ocean. On the other hand, the role of CLLJ coupled with the Pacific jet aloft is notable in the moisture transport to the Gulf coastal plains. The CLLJ merges with the strong westerlies associated with the Pacific jet aloft, and steers along the east coast of the Gulf of Mexico, transporting moisture to the lower Mississippi basin where it connects with the GPLLJ. This phenomenon, dubbed the "Maya Express", has been previously reported in connection with the warm season flooding in the Midwest US (Dirmeyer and Kinter, 2010, 2009) and closely matches with the moisture advection mechanisms reported in (Debbage et al., 2017). This is also indicative of a higher moisture flux distributed throughout the lower tropospheric column that highly increases the chance of very heavy rainfall if sufficient convective available potential energy (CAPE) is present (Rabinowitz et al., 2019). The transport of moisture to these regions are dominated by two distinct branches of LLJ propagation that can be seen to become stronger during 2-0 days from the event occurrences, thereby, confirming a cascading effect of the synoptic patterns on the moisture transportation by ARs into the region (Fig. 5(d-f)).

Furthermore, the southeastern coastal plains are shown to exhibit an intense stationary low-pressure system associated with the warm season AR-EPs (Fig. 5(d-f)). The persistent low-pressure structure favors deep moist convection leading to more severe warm-season AR-EPs in the region (Moore et al., 2015; Nie and Fan, 2019). This is further reinforced by the relatively greater moisture availability associated with the warm-season AR-EPs as indicated by the significantly (13–16 mm) higher positive anomalies of TCWV on the days of the events (Fig. 6(i)). The linkages between the spatial evolution of the moisture advection mechanisms and AR-related precipitation events are in close agreement with previous studies that identify the Gulf of Mexico as the primary source of moisture. This highlights the role of CLLJ and the Pacific jet aloft in the advection of moisture into the region (Debbage et al., 2017; Dirmeyer and Kinter, 2010, 2009; Lavers and Villarini, 2013b; Moore et al., 2011; Rabinowitz et al., 2019).

Overall, the evolution of the source of moisture and its advection associated with the warm and cold season AR-EP events suggest the presence of a cascading effect from the synoptic-scale meteorological patterns (exhibited by the evolution of MSLP and Z850 composite anomalies in Fig. 5). Our results produce new information related to the sequential development of available moisture and advection processes associated with ARs that finally lead to the most severe EP events in the SEUS region. The cold season AR-EPs are more frequent and driven by relatively stronger dynamical systems indicated by greater IVT intensity. On the other hand, the warm season AR-EPs are more severe and caused by higher atmospheric instability and more moist conditions characterized by stationary low-pressure structures and higher TCWV anomalies.

4. Synthesis and conclusion

We investigated the cascading impact of synoptic-scale atmospheric patterns on the advection mechanisms linked to the atmospheric riverrelated extreme precipitation events in the Coastal South East US (SEUS). Spatiotemporal variation of the AR-EP event suggests a strong seasonal dependence across most states in the SEUS region. While a greater number of AR-EP events are observed during the cold season, the events are found to be more severe in the warm season. The spatiotemporal evolution of relevant synoptic features suggested a strong cascading effect on the key mechanisms (moisture availability and mode

of advection) that drive the occurrence of AR-EP events during the warm and cold seasons in the SEUS region. The following conclusions can be drawn from this study.

- (a) Overall, 14,992 landfalling ARs were detected (after removing the TCs) from 1979 to 2019. Compared to the warm seasons, a relatively greater number of AR-activities were observed during the cold seasons. The maximum (12–15) number of AR events per year was reported for the SEUS region's easternmost states. These regions experience 11–16 EP_{95p}, and 3–5 EP_{99p} events per year.
- (b) The higher number of AR-EP events were observed along the northwestern coast of the Florida peninsula and south of Georgia. In addition to that, about 3–5 AR-EP_{99p} and at least 1–2 AR-EP_{99p} events per year are found to occur in the entire eastern part of the SEUS region. Seasonal counts of AR-EP event occurrences and average precipitation magnitudes showed a pronounced seasonal dependence. Fifty AR-EP_{95p} and twelve AR-EP_{99p} events were observed over Georgia, Florida, Alabama, and South Carolina during the OND, NDJ, DJF, JFM, FMA, and MAM seasons. Only a few AR-EP events (less than 5–10 events) are found to occur during the extended warm season months (AMJ to SON) over the entire SEUS region. On the other hand, the average precipitation magnitude of the AR-EP_{95p} and AR-EP_{99p} events is found to be relatively greater (55–90 mm/day) in the warm seasons.
- (c) The evolution of Z850 anomalies associated with the cold season AR-EP events suggested several troughs and ridge formations across much of the Central Plains and the Gulf Coastal plains. These regions are characterized by a zone of enhanced geostrophic winds indicating highly anomalous weather conditions. On the other hand, the warm season anomalies indicated a gradual strengthening of a persistent low-pressure system (2 days before the event timings) resembling that of cut-off lows in the region (covering much of the Gulf coastal plains) that might trigger enhancement of heavy rainfall events in the presence of ARs. The spatiotemporal evolution of the composite anomalies in MSLP, associated with the cold season top 100 AR-EP events, exhibited strengthening of a pressure dipole with an eastward extension of the Bermuda high- and a high-pressure center over the western US.
- (d) The moisture transport depicted by the composites of the IVT field associated with both the cold and warm season AR-EP events are found to mimic the spatiotemporal evolution of the MSLP and Z850 composites for the respective seasons. During the cold (warm) season, IVT intensity gradually strengthens 2 days (5-days, 2-days) prior to the events and steer over the SEUS region, finally moving up to the Atlantic Ocean. However, compared to the cold season, the warm season AR-EPs are associated with relatively weaker IVT strength. In addition to that, relatively moister conditions were found to be associated with the warm season AR-EPs, which is indicated by significantly higher TCWV anomalies over the affected region. The marked increase in moisture availability is attributed to the slowly varying background circulations that favor deep moist convection leading to more severe warm-season EPs in the region (Moore et al., 2015; Nie and Fan, 2019). Such spatiotemporal evolution confirmed the cascading effect of synoptic patterns on the moisture availability and mode of advection associated with AR-EP events in the SEUS region.

The results from this study are expected to provide adequate understanding and background that will help predict future AR-EP events in the SEUS region. The seasonal AR characteristics presented here may be extended further to assess the seasonal water cycle influenced by ARs in the region, which can significantly aid in the advanced planning and management of water resources related to ARs. The synoptic meteorological characteristics discussed in this study can be used as important priors to design early warning and management systems related to AR-driven floods in the SEUS. Future research will aim to address the uncertainties associated with the detection of ARs in the region (Rutz et al., 2019; Shields et al., 2018a), the impact of other modes of climate variabilities, or if global warming plays a significant role in modulating the statistical behavior or time of emergence of ARs in the SEUS. The possible impact of monsoon ridges on the precipitation variability and

its coupling with the large scale climate variabilities (Khedun et al., 2014), or the combined impact of occurrence, intensity, and duration of ARs (Chen et al., 2018) can be examined. There is also a need to explore the interplay between the ARs and other physical mechanisms such as CAPE (Rabinowitz et al., 2019) and the presence of cut-off lows (Tsuji and Takayabu, 2019) in a more direct fashion that could bridge specific knowledge gaps.

Declaration of Competing Interest

The authors declare that they have no known competing financial interests or personal relationships that could have appeared to influence the work reported in this paper.

Acknowledgment

This study was supported by the National Science Foundation (NSF) award # 1855374. We are thankful for the data provided by the NOAA Climate Prediction Centre (NOAA CPC; http://www.cpc.ncep.noaa.gov/), and high-resolution European Centre for Medium-Range Weather Forecasts Reanalysis 5 (ERA5). Additionally, we thank editor, Dr. Sally Elizabeth Thompson, and the reviewers for their valuable and constructive feedback to improve the original manuscript.

Appendix A. Supplementary data

Supplementary data to this article can be found online at https://doi.org/10.1016/j.jhydrol.2021.126641.

References

- Barbero, R., Abatzoglou, J.T., Fowler, H.J., 2019. Contribution of large-scale midlatitude disturbances to hourly precipitation extremes in the United States. Clim. Dyn. 52 (1-2), 197–208. https://doi.org/10.1007/s00382-018-4123-5.
- Barlow, M., Gutowski, W.J., Gyakum, J.R., Katz, R.W., Lim, Y.-K., Schumacher, R.S., Wehner, M.F., Agel, L., Bosilovich, M., Collow, A., Gershunov, A., Grotjahn, R., Leung, R., Milrad, S., Min, S.-K., 2019. North American extreme precipitation events and related large-scale meteorological patterns: a review of statistical methods, dynamics, modeling, and trends. Clim. Dyn. 53 (11), 6835–6875. https://doi.org/10.1007/s00382-019-04958-z.
- Barth, N.A., Villarini, G., Nayak, M.A., White, K., 2017. Mixed populations and annual flood frequency estimates in the western United States: the role of atmospheric rivers. Water Resour. Res. 53 (1), 257–269. https://doi.org/10.1002/ 2016WR019064.
- Chen, M., Shi, W., Xie, P., Silva, V.B.S., Kousky, V.E., Wayne Higgins, R., Janowiak, J.E., 2008. Assessing objective techniques for gauge-based analyses of global daily precipitation. J. Geophys. Res.: Atmospheres 113 (D4). https://doi.org/10.1029/2007JD009132.
- Chen, X., Leung, L.R., Gao, Y., Liu, Y., Wigmosta, M., Richmond, M., 2018. Predictability of extreme precipitation in Western U.S. Watersheds based on atmospheric river occurrence, intensity, and duration. Geophys. Res. Lett. 45, 11693–11701. https:// doi.org/10.1029/2018GL079831.
- Chen, X., Leung, L.R., Wigmosta, M., Richmond, M., 2019. Impact of atmospheric rivers on surface hydrological processes in Western U.S. Watersheds. J. Geophys. Res.: Atmospheres 124 (16), 8896–8916. https://doi.org/10.1029/2019JD030468.
- Corringham, T.W., Ralph, F.M., Gershunov, A., Cayan, D.R., Talbot, C.A., 2019. Atmospheric rivers drive flood damages in the western United States. Sci. Adv. 5 (12), eaax4631. https://doi.org/10.1126/sciadv.aax4631.
- Debbage, N., Miller, P., Poore, S., Morano, K., Mote, T., Marshall Shepherd, J., 2017. A climatology of atmospheric river interactions with the southeastern United States coastline. Int. J. Climatol. 37 (11), 4077–4091. https://doi.org/10.1002/joc.2017.37.issue-1110.1002/joc.5000.
- Dettinger, M., 2011. Climate change, atmospheric rivers, and floods in California a multimodel analysis of storm frequency and magnitude changes. JAWRA J. Am. Water Resour. Assoc. 47, 514–523. https://doi.org/10.1111/j.1752-1688.2011.00546.x.
- Dettinger, M.D., 2013. Atmospheric rivers as drought busters on the U.S. West Coast. J. Hydrometeor. 14, 1721–1732. https://doi.org/10.1175/JHM-D-13-02.1.
- Dettinger, M.D., Ralph, F.M., Das, T., Neiman, P.J., Cayan, D.R., 2011. Atmospheric rivers, floods and the water resources of California. Water 3, 445–478. https://doi. org/10.3390/w3020445.
- Dirmeyer, P.A., Kinter, J.L., 2010. Floods over the U.S. Midwest: a regional water cycle perspective. J. Hydrometeor. 11, 1172–1181. https://doi.org/10.1175/ 2010.JHM1196.1.
- Dirmeyer, P.A., Kinter, J.L., 2009. The "maya express": floods in the U.S. Midwest. Eos, Trans. Am. Geophys. Union 90 (12), 101–102. https://doi.org/10.1029/ 2009E0120001.

- Gimeno, L., Nieto, R., Vázquez, M., Lavers, D.A., 2014. Atmospheric rivers: a minireview. Front. Earth Sci. 2 https://doi.org/10.3389/feart.2014.00002.
- Gimeno, L., Stohl, A., Trigo, R.M., Dominguez, F., Yoshimura, K., Yu, L., Drumond, A., Durán-Quesada, A.M., Nieto, R., 2012. Oceanic and terrestrial sources of continental precipitation. Rev. Geophys. 50 (4) https://doi.org/10.1029/2012RG000389.
- Guan, B., Molotch, N.P., Waliser, D.E., Fetzer, E.J., Neiman, P.J., 2010. Extreme snowfall events linked to atmospheric rivers and surface air temperature via satellite measurements. Geophys. Res. Lett. 37 (20) https://doi.org/10.1029/ 2010GI.044696.
- Guan, B., Waliser, D.E., 2015. Detection of atmospheric rivers: Evaluation and application of an algorithm for global studies. J. Geophys. Res. arch: Atmospheres 120 (24), 12514–12535. https://doi.org/10.1002/2015JD024257.
- Guirguis, K., Gershunov, A., Shulgina, T., Clemesha, R.E.S., Ralph, F.M., 2019. Atmospheric rivers impacting Northern California and their modulation by a variable climate. Clim. Dyn. 52 (11), 6569–6583. https://doi.org/10.1007/s00382-018-4532-5.
- Huning, L.S., Guan, B., Waliser, D.E., Lettenmaier, D.P., 2019. Sensitivity of seasonal snowfall attribution to atmospheric rivers and their reanalysis-based detection. Geophys. Res. Lett. 46 (2), 794–803. https://doi.org/10.1029/2018GL080783.
- Kamae, Y., Mei, W., Xie, S.-P., Naoi, M., Ueda, H., 2017. Atmospheric Rivers over the northwestern pacific: climatology and interannual variability. J. Climate 30 (15), 5605–5619. https://doi.org/10.1175/JCLI-D-16-0875.1.
- Khedun, C.P., Mishra, A.K., Singh, V.P., Giardino, J.R., 2014. A copula-based precipitation forecasting model: Investigating the interdecadal modulation of ENSO's impacts on monthly precipitation. Water Resour. Res. 50 (1), 580–600. https://doi.org/10.1002/wrcr.v50.110.1002/2013WR013763.
- Kim, J., Guan, B., Waliser, D.E., Ferraro, R.D., Case, J.L., Iguchi, T., Kemp, E., Putman, W., Wang, W., Wu, D., Tian, B., 2018. Winter precipitation characteristics in western US related to atmospheric river landfalls: observations and model evaluations. Clim. Dyn. 50 (1-2), 231–248. https://doi.org/10.1007/s00382-017-3601-5
- Knight, D.B., Davis, R.E., 2009. Contribution of tropical cyclones to extreme rainfall events in the southeastern United States. J. Geophys. Res.: Atmos. 114 (D23) https://doi.org/10.1029/2009JD012511.
- Lamjiri, M.A., Dettinger, M.D., Ralph, F.M., Guan, B., 2017. Hourly storm characteristics along the U.S. West Coast: role of atmospheric rivers in extreme precipitation. Geophys. Res. Lett. 44 (13), 7020–7028. https://doi.org/10.1002/2017GL074193.
- Lavers, D.A., Villarini, G., 2013a. The nexus between atmospheric rivers and extreme precipitation across Europe. Geophys. Res. Lett. 40 (12), 3259–3264. https://doi. org/10.1002/grl.50636.
- Lavers, D.A., Villarini, G., 2013b. Atmospheric rivers and flooding over the central United States. J. Climate 26, 7829–7836. https://doi.org/10.1175/JCLI-D-13-00212.1.
- Lavers, D.A., Villarini, G., Allan, R.P., Wood, E.F., Wade, A.J., 2012. The detection of atmospheric rivers in atmospheric reanalyses and their links to British winter floods and the large-scale climatic circulation. J. Geophys. Res.: Atmospheres 117 (D20). https://doi.org/10.1029/2012JD018027.
- Madsen, H., Lawrence, D., Lang, M., Martinkova, M., Kjeldsen, T.R., 2014. Review of trend analysis and climate change projections of extreme precipitation and floods in Europe. J. Hydrol. 519, 3634–3650. https://doi.org/10.1016/j.jhydrol.2014.11.003.
- Mahoney, K., Jackson, D.L., Neiman, P., Hughes, M., Darby, L., Wick, G., White, A., Sukovich, E., Cifelli, R., 2016. Understanding the role of atmospheric rivers in heavy precipitation in the southeast United States. Mon. Wea. Rev. 144, 1617–1632. https://doi.org/10.1175/MWR-D-15-0279.1.
- Maurer, E.P., Wood, A.W., Adam, J.C., Lettenmaier, D.P., Nijssen, B., 2002. A Long-term hydrologically based dataset of land surface fluxes and states for the conterminous United States. J. Climate 15, 3237–3251. https://doi.org/10.1175/1520-0442 (2002)015<3237:ALTHBD>2.0.CO:2.
- Miller, D.K., Hotz, D., Winton, J., Stewart, L., 2017. Investigation of atmospheric rivers impacting the pigeon river basin of the southern appalachian mountains. Wea. Forecast. 33, 283–299. https://doi.org/10.1175/WAF-D-17-0060.1.
- Mishra, A.K., Singh, V.P., 2010. Changes in extreme precipitation in Texas. J. Geophys. Res.: Atmospheres 115 (D14). https://doi.org/10.1029/2009JD013398.
- Mondal, S., Mishra, A.K., Leung, L.R., 2020. Spatiotemporal characteristics and propagation of summer extreme precipitation events over United States: a complex network analysis. Geophys. Res. Lett. 47, e2020GL088185. https://doi.org/ 10.1029/2020GL088185.
- Moore, B.J., Mahoney, K.M., Sukovich, E.M., Cifelli, R., Hamill, T.M., 2015. Climatology and environmental characteristics of extreme precipitation events in the southeastern United States. Mon. Weather Rev. 143, 718–741. https://doi.org/ 10.1175/MWR-D-14-00065.1.
- Moore, B.J., Neiman, P.J., Ralph, F.M., Barthold, F.E., 2011. Physical processes associated with heavy flooding rainfall in Nashville, Tennessee, and vicinity during 1–2 May 2010: the role of an atmospheric river and mesoscale convective systems. Mon. Wea. Rev. 140 (2), 358–378. https://doi.org/10.1175/MWR-D-11-00126.1.
- Mundhenk, B.D., Barnes, E.A., Maloney, E.D., 2016. All-season climatology and variability of atmospheric river frequencies over the north pacific. J. Climate 29, 4885–4903. https://doi.org/10.1175/JCLI-D-15-0655.1.
- Neiman, P.J., Ralph, F.M., Wick, G.A., Kuo, Y.-H., Wee, T.-K., Ma, Z., Taylor, G.H., Dettinger, M.D., 2008a. Diagnosis of an intense atmospheric river impacting the Pacific Northwest: storm summary and offshore vertical structure observed with COSMIC satellite retrievals. Mon. Wea. Rev. 136, 4398–4420. https://doi.org/ 10.1175/2008MWR2550.1.
- Neiman, P.J., Ralph, F.M., Wick, G.A., Lundquist, J.D., Dettinger, M.D., 2008b. Meteorological characteristics and overland precipitation impacts of atmospheric rivers affecting the West Coast of North America based on eight years of SSM/I

- satellite observations. J. Hydrometeor. 9, 22–47. https://doi.org/10.1175/
- Newell, R.E., Newell, N.E., Zhu, Y., Scott, C., 1992. Tropospheric rivers? a pilot study. Geophys. Res. Lett. 19 (24), 2401–2404. https://doi.org/10.1029/92GL02916.
- Nie, J., Fan, B., 2019. Roles of dynamic forcings and diabatic heating in summer extreme precipitation in East China and the southeastern United States. J. Climate 32, 5815–5831. https://doi.org/10.1175/JCLI-D-19-0188.1.
- Paltan, H., Waliser, D., Lim, W.H., Guan, B., Yamazaki, D., Pant, R., Dadson, S., 2017. Global floods and water availability driven by atmospheric rivers. Geophys. Res. Lett. 44 (20), 10,387–10,395. https://doi.org/10.1002/2017GL074882.
- Papalexiou, S.M., Montanari, A., 2019. Global and regional increase of precipitation extremes under global warming. Water Resour. Res. 55, 4901–4914. https://doi.org/ 10.1029/2018WR024067
- Parker, M.D., Ahijevych, D.A., 2007. Convective episodes in the east-central United States. Mon. Wea. Rev. 135, 3707–3727. https://doi.org/10.1175/ 2007AMB 2009 1.
- Pasquier, J.T., Pfahl, S., Grams, C.M., 2019. Modulation of atmospheric river occurrence and associated precipitation extremes in the North Atlantic region by European Weather regimes. Geophys. Res. Lett. 46 (2), 1014–1023. https://doi.org/10.1029/ 2018/2104
- Payne, A.E., Demory, M.-E., Leung, L.R., Ramos, A.M., Shields, C.A., Rutz, J.J., Siler, N., Villarini, G., Hall, A., Ralph, F.M., 2020. Responses and impacts of atmospheric rivers to climate change. Nat. Rev. Earth Environ. 1 (3), 143–157. https://doi.org/ 10.1038/s43017-020-0030-5
- Pfahl, S., Madonna, E., Boettcher, M., Joos, H., Wernli, H., 2013. Warm conveyor belts in the ERA-interim dataset (1979–2010). Part II: moisture origin and relevance for precipitation. J. Climate 27, 27–40. https://doi.org/10.1175/JCLI-D-13-00223.1.
- Porter, K., Wein, A., Alpers, C., Baez, A., Barnard, P., Carter, J., Corsi, A., Costner, J., Cox, D., Das, T., 2011. Overview of the ARkStorm scenario: U.S. Geological Survey Open-File Report 2010-1312, 183 p. and appendixes. Hanh, Mitchell, David, Morman, Suzette, Neiman, Paul, Olsen, Anna, Perry, Suzanne, Plumlee, Geoffrey, Ralph, Martin, Reynolds, David, Rose, Adam, Schaefer, Kathleen, Serakos, Julie, Siembieda, William, Stock, Jonathan, Strong, David, Sue Wing, Ian, Tang, Alex, Thomas, Pete, Topping, Ken, and Wills, Chris 2010–1312.
- Rabinowitz, J.L., Lupo, A.R., Market, P.S., Guinan, P.E., 2019. An investigation of atmospheric rivers impacting heavy rainfall events in the North-Central Mississippi River Valley. Int. J. Climatol. 39 (10), 4091–4106. https://doi.org/10.1002/ ioc.6061
- Ralph, F.M., Coleman, T., Neiman, P.J., Zamora, R.J., Dettinger, M.D., 2013. Observed impacts of duration and seasonality of atmospheric-river landfalls on soil moisture and runoff in Coastal Northern California. J. Hydrometeorol. 14, 443–459. https:// doi.org/10.1175/JHM-D-12-076.1.
- Ralph, F.M., Dettinger, M.D., 2011. Historical and national perspectives on extreme west coast precipitation associated with atmospheric rivers during December 2010. Bull. Amer. Meteor. Soc. 93 (6), 783–790. https://doi.org/10.1175/BAMS-D-11-00188.1.
- Ralph, F.M., Neiman, P.J., Wick, G.A., 2004. Satellite and CALJET aircraft observations of atmospheric rivers over the eastern north pacific ocean during the Winter of 1997/98. Mon. Wea. Rev. 132, 1721–1745. https://doi.org/10.1175/1520-0493 (2004)132<1721:SACAOO>2.0.CO:2.
- Ralph, F.M., Neiman, P.J., Wick, G.A., Gutman, S.I., Dettinger, M.D., Cayan, D.R., White, A.B., 2017. Flooding on California's Russian River: role of atmospheric rivers. Geophys. Res. Lett. 33 (13) https://doi.org/10.1029/2006GL026689.
- Ralph, F.M., Rutz, J.J., Cordeira, J.M., Dettinger, M., Anderson, M., Reynolds, D., Schick, L.J., Smallcomb, C., 2019. A scale to characterize the strength and impacts of atmospheric rivers. Bull. Am. Meteorol. Soc. 100, 269–289. https://doi.org/ 10.1175/BAMS-D-18-0023.1.
- Ramos, A.M., Trigo, R.M., Liberato, M.L.R., Tomé, R., 2015. Daily precipitation extreme events in the Iberian Peninsula and its association with atmospheric rivers. J. Hydrometeor. 16, 579–597. https://doi.org/10.1175/JHM-D-14-0103.1.
- Rickenbach, T., 2018. Seasonal changes of extremes in isolated and mesoscale precipitation for the Southeastern United States. Atmosphere 9, 309. https://doi. org/10.3390/atmos9080309.
- Ridder, N., de Vries, H., Drijfhout, S., 2018. The role of atmospheric rivers in compound events consisting of heavy precipitation and high storm surges along the Dutch coast.

- Nat. Hazards Earth Syst. Sci. 18 (12), 3311–3326. https://doi.org/10.5194/nhess-18-3311-2018.
- Rutz, J.J., Shields, C.A., Lora, J.M., Payne, A.E., Guan, B., Ullrich, P., O'Brien, T., Leung, L.R., Ralph, F.M., Wehner, M., Brands, S., Collow, A., Goldenson, N., Gorodetskaya, I., Griffith, H., Kashinath, K., Kawzenuk, B., Krishnan, H., Kurlin, V., Lavers, D., Magnusdottir, G., Mahoney, K., McClenny, E., Muszynski, G., Nguyen, P. D., Prabhat, M.r., Qian, Y., Ramos, A.M., Sarangi, C., Sellars, S., Shulgina, T., Tome, R., Waliser, D., Walton, D., Wick, G., Wilson, A.M., Viale, M., 2019. The atmospheric river tracking method intercomparison project (ARTMIP): quantifying uncertainties in atmospheric river climatology. J. Geophys. Res.: Atmos. 124 (24), 13777–13802. https://doi.org/10.1029/2019JD030936.
- Rutz, J.J., Steenburgh, W.J., Ralph, F.M., 2013. Climatological characteristics of atmospheric rivers and their inland penetration over the Western United States. Mon. Wea. Rev. 142, 905–921. https://doi.org/10.1175/MWR-D-13-00168.1.
- Schumacher, R.S., Rasmussen, K.L., 2020. The formation, character and changing nature of mesoscale convective systems. Nat. Rev. Earth Environ. 1 (6), 300–314. https:// doi.org/10.1038/s43017-020-0057-7.
- Shields, C.A., Rutz, J.J., Leung, L.R., Ralph, F.M., Wehner, M., O'Brien, T., Pierce, R., 2018a. Defining Uncertainties through Comparison of Atmospheric River Tracking Methods. Bull. Amer. Meteor. Soc. 100, ES93–ES96. https://doi.org/10.1175/BAMS-D-18-0200.1.
- Shields, C.A., Rutz, J.J., Leung, L.-Y., Ralph, F.M., Wehner, M., Kawzenuk, B., Lora, J.M., McClenny, E., Osborne, T., Payne, A.E., Ullrich, P., Gershunov, A., Goldenson, N., Guan, B., Qian, Y., Ramos, A.M., Sarangi, C., Sellars, S., Gorodetskaya, I., Kashinath, K., Kurlin, V., Mahoney, K., Muszynski, G., Pierce, R., Subramanian, A.C., Tome, R., Waliser, D., Walton, D., Wick, G., Wilson, A., Lavers, D., Collow, A., Krishnan, H., Magnusdottir, G., Nguyen, P., 2018b. Atmospheric river tracking method intercomparison project (ARTMIP): project goals and experimental design. Geosci. Model Dev. 11 (6), 2455–2474. https://doi.org/10.5194/gmd-11-2455-2018-supplement.
- Steinschneider, S., Ho, M., Williams, A.P., Cook, E.R., Lall, U., 2018. A 500-year tree ring-based reconstruction of extreme cold-season precipitation and number of atmospheric river landfalls across the Southwestern United States. Geophys. Res. Lett. 45 (11), 5672–5680. https://doi.org/10.1029/2018GL078089.
- Tsuji, H., Takayabu, Y.N., 2019. Precipitation enhancement via the interplay between atmospheric rivers and cutoff lows. Mon. Wea. Rev. 147, 2451–2466. https://doi. org/10.1175/MWR-D-18-0358.1.
- Valenzuela, R.A., Garreaud, R.D., 2019. Extreme daily rainfall in central-southern chile and its relationship with low-level horizontal water vapor fluxes. J. Hydrometeor. 20, 1829–1850. https://doi.org/10.1175/JHM-D-19-0036.1.
- Vu, T.M., Mishra, A.K., 2019. Nonstationary frequency analysis of the recent extreme precipitation events in the United States. J. Hydrol. 575, 999–1010. https://doi.org/ 10.1016/j.jhydrol.2019.05.090
- Waliser, D., Guan, B., 2017. Extreme winds and precipitation during landfall of atmospheric rivers. Nat. Geosci 10 (3), 179–183. https://doi.org/10.1038/ prec/3804
- Wang, C., Lee, S.-k., 2007. Atlantic warm pool, Caribbean low-level jet, and their potential impact on Atlantic hurricanes. Geophys. Res. Lett. 34 (2) https://doi.org/ 10.1029/2006GL028579
- Wang, D., Hagen, S.C., Alizad, K., 2013. Climate change impact and uncertainty analysis of extreme rainfall events in the Apalachicola River basin, Florida. J. Hydrol. 480, 125–135. https://doi.org/10.1016/j.jhydrol.2012.12.015.
- Wen, J., Chen, J., Lin, W., Jiang, B., Xu, S., Lan, J., 2020. Impacts of anthropogenic heat flux and urban land-use change on frontal rainfall near coastal regions: a case study of a rainstorm over the pearl river Delta, South China. J. Appl. Meteor. Climatol. 59, 363–379. https://doi.org/10.1175/JAMC-D-18-0296.1.
- Zhang, Z., Ralph, F.M., Zheng, M., 2019. The relationship between extratropical cyclone strength and atmospheric river intensity and position. Geophys. Res. Lett. 46 (3), 1814–1823. https://doi.org/10.1029/2018GL079071.
- Zhu, Y., Newell, R.E., 1998. A proposed algorithm for moisture fluxes from atmospheric rivers. Mon. Wea. Rev. 126, 725–735. https://doi.org/10.1175/1520-0493(1998) 126<0725:APAFMF>2.0.CO;2.